Supplement of Nat. Hazards Earth Syst. Sci., 26, 1075–1104, 2026
https://doi.org/10.5194/nhess-26-1075-2026-supplement

Natural Hazards and Earth System Sciences
Open Access
EGU

Supplement of

Harnessing multi-source hydro-meteorological data for high flows modelling in a partially glacierized Himalayan basin

Domenico De Santis et al.

Correspondence to: Domenico De Santis (domenico.desantis@cnr.it)

S1. MISDc-2L model description and implementation

MISDc-2L model (Brocca et al., 2011, 2012; Massari et al., 2018) reproduces several hydrological processes and different runoff generation mechanisms. It simulates the temporal evolution of soil moisture in an upper (layer 1) and lower (layer 2) soil storage, expressed as water depth W and limited to $W_{\max,1}$ and $W_{\max,2}$, respectively. This two-layer approach allows describing the different controls of soil moisture on the partitioning of water input into infiltration and surface runoff (infiltration excess, IE) at the upper layer, as well as the saturation excess (SE) occurring when water content exceeds the capacity of one or both soil storages. The following relationships regulate actual (AET) to potential evapotranspiration (PET) ratio, infiltration-surface runoff partitioning, and percolation rate from each of the two layers ($P_{r,1}$ and $P_{r,2}$):

$$\mathrm{AET} = \mathrm{PET}\frac{W}{W_{\max}} \quad \text{(S1)}$$

$$\mathrm{IE} = (R + M)\left(\frac{W_1}{W_{\max,1}}\right)^{\alpha} \quad \text{(S2)}$$

$$P_{r,i} = K_{s,i}\left(\frac{W_i}{W_{\max,i}}\right)^{m_i} \quad \text{(S3)}$$

where IE is related to the water input due to rainfall R and meltwater M from snowpack and glaciers, while α, $K_{s,1}$, m_1, $K_{s,2}$, and m_2 are parameters to be calibrated. Different assumptions can be made about the reference soil moisture for the evapotranspiration demand, generally resulting in contributions from both soil layers.

Surface runoff generated from infiltration and saturation excess is then convoluted through a Geomorphological Instantaneous Unit Hydrograph (GIUH), while subsurface runoff due to percolation from the lower layer is transferred via a linear reservoir approach.

The modelled streamflow at sub-basin outlet is then propagated in the downstream channel network according to a diffusive wave approach without lateral inflows (Brocca et al., 2011). At sub-basin scale, the incoming streamflow in the upstream section $Q(0, t)$ is convoluted to the outlet via the following relationship:

$$Q(L,t) = Q(0,t) \otimes \left[\frac{L}{2\sqrt{\pi D t^3}} exp\left(-\frac{(L-ct)^2}{4Dt}\right)\right] \quad \text{(S4)}$$

where L is the stream length [m] derived from the digital elevation model (DEM), t is the time [s], c is the celerity [m/s], and D is the diffusion coefficient [m^2/s].

In this application, empirical relationships between river basin and streamflow response characteristics were considered to parsimoniously represent the spatial variability of convolution and propagation parameters across sub-basins (e.g., Alexander, 1982; Bentura & Michel, 1997). Such an approach allows to fix a priori a relative spatial pattern of a parameter, while allowing to modify its local magnitude by calibrating the lumped coefficients of these relationships (e.g., Andersen et al., 2001; Francés et al., 2007).

Parameters of geomorphological and linear reservoir IUH were related with the sub-basin area, considering a scaling exponent value reported in previous studies (e.g., Melone et al., 2002; Schaefli et al., 2014):

$$t_L = \gamma_{\mathrm{GIUH}} \cdot A^{0.33} \quad \text{(S5)}$$

$$k_{\mathrm{LR}} = \gamma_{\mathrm{LR}} \cdot A^{0.33} \quad \text{(S6)}$$

where t_L is the GIUH lag time [h], k_{LR} is the linear reservoir parameter [h], A is the sub-basin area [km^2], and γ_{GIUH} and γ_{LR} are lumped parameters to be calibrated (with the latter expected higher than the former).

Parameters in Eq. (S4) were related with the stream slope at sub-basin scale, obtained from the DEM. The following relationships have been proposed here, derived from theoretical and parameter parsimony considerations:

$$c = k_c \cdot s^{0.5} \quad \text{(S7)}$$

$$D = k_D \cdot s^{-1} \quad \text{(S8)}$$

where s is the stream slope and k_c and k_D are lumped parameters to be calibrated.

In the original applications of the model (e.g., Brocca et al., 2011), a common parameter was used to control both GIUH and linear reservoir responses, while c and D were lumped within the basin.

The structure of the general model implemented for this study at sub-basin scale is represented at the end of this section.

Regarding the model forcings, PET was calculated from the reference evapotranspiration ET_0 through a lumped coefficient to be calibrated:

$$PET = k_{PET} \cdot ET_0 \quad \text{(S9)}$$

while the several adjustments of the precipitation P are described in the main text, as well as the methods which regulates snowpack (S_p) storage evolution, i.e. separation between rainfall and snowfall (S_f) and snow melting (S_{melt}). Ice melting from glacierized areas (I_{melt}) is assumed to occur once the snowpack is locally depleted. In this application, the spatial matching between ERA5-Land grid points and sub-basins was carried out assigning the latter a 3-km buffer. Similarly, a 500-m buffer applied to glaciers was used to identify meteorological nodes at the sub-basin scale on which to represent ice melt in addition to snow melt. Reference altitude of ERA5-Land grid cells was derived from the geopotential height.

Following a common simplification in conceptual hydrological models (e.g., Schaefli et al., 2005, 2014), the contribution to evapotranspiration demand does not come from snowpack (or glaciers), thus neglecting the sublimation process in favour of the melting one. It is noteworthy that, in this application, independent AET data were used to constrain the simulation, with the overall volume of modelled AET mimicking the reference value, so neglecting sublimation has no effect on the water budget.

Finally, $W_{max,1}$ and $W_{max,2}$ were not calibrated but set at 500 and 3000 mm, respectively, to limit overparameterization issues. It was assumed that evapotranspiration is sustained only by layer 1 given the depth of the latter (which corresponds to 1 m soil depth by considering a porosity value of 0.5 m^3 m^{-3}). The water depth in snowpack storage was assumed null at the start of the model warmup, while in the upper and lower soil storages it was set to half of their total thickness.

For model calibration, a single-objective global optimization algorithm was applied, specifically the Covariance Matrix Adaptation Evolution Strategy, CMA-ES (Hansen et al., 2003). Several CMA-ES control settings were not altered from their defaults, except for three termination criteria. Specifically, “TolFun” and “TolX”, which are mainly associated with the objective function values and the standard deviation of the normal distribution used to sample the parameter values, respectively, were set at 10^{-4}. Furthermore, the maximal number of function evaluations (“MaxFunEvals”) was fixed at 10^5. The model parameters were encoded in the range [0; 10] so that they would presumably have similar sensitivity. For this purpose, a linear or logarithmic transformation was used, depending on the original parameter range. For each parameter, the initial solution point was generally chosen equal to the intermediate value (i.e., 5), and the initial standard deviation for the sampling distributions was set to one-third of the parameter range (i.e., ≈ 3.33).

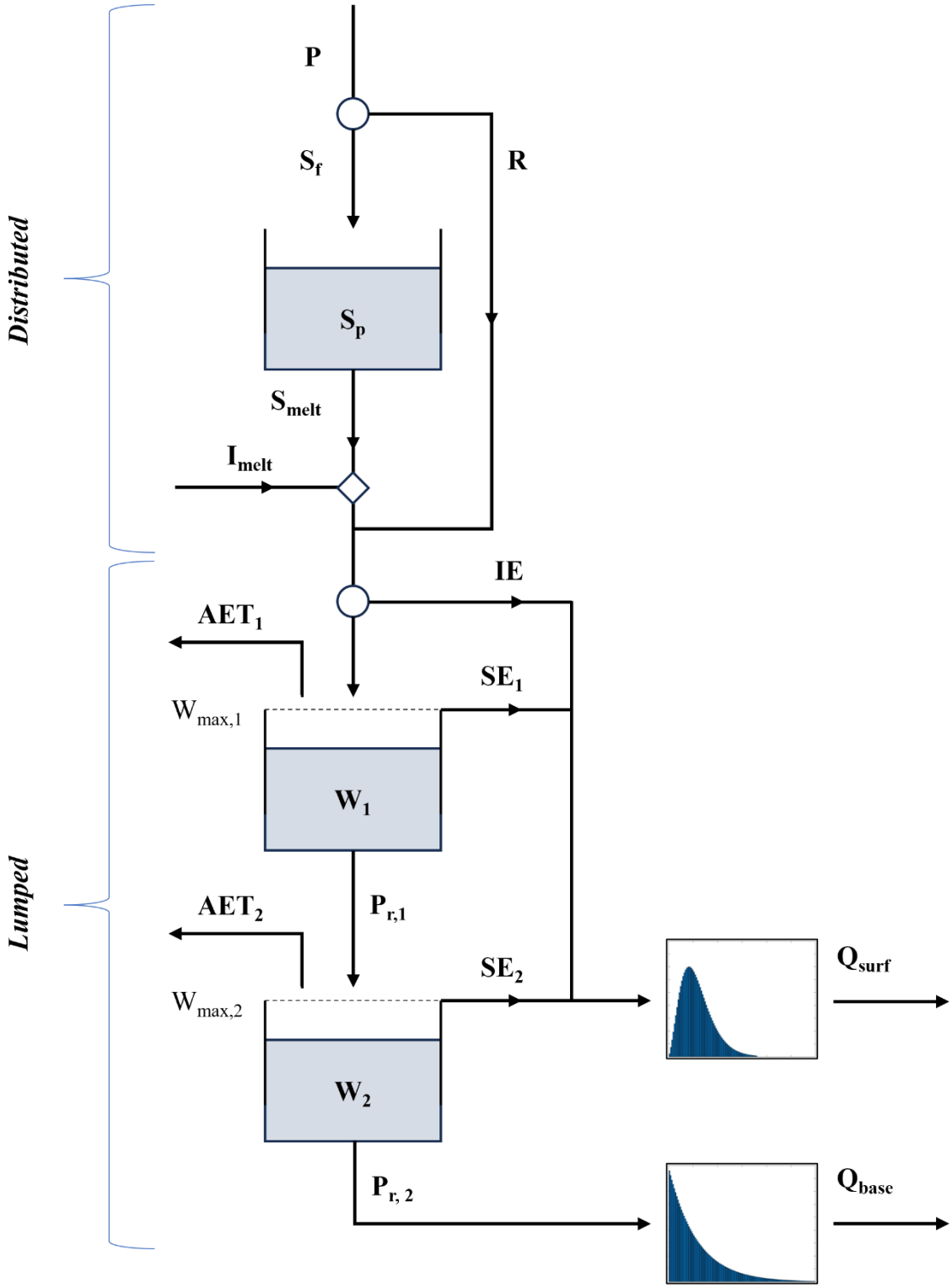

General structure of the model described in this study

REFERENCES

Alexander, G. (1972). Effect of catchment area on flood magnitude. *Journal of Hydrology*, *16*(3), 225–240. https://doi.org/10.1016/0022-1694(72)90054-6

Andersen, J., Refsgaard, J. C., & Jensen, K. H. (2001). Distributed hydrological modelling of the Senegal River Basin — model construction and validation. *Journal of Hydrology*, *247*(3–4), 200–214. https://doi.org/10.1016/s0022-1694(01)00384-5

Bentura, P. L. F., & Michel, C. (1997). Flood routing in a wide channel with a quadratic lag-and-route method. *Hydrological Sciences Journal*, *42*(2), 169–189. https://doi.org/10.1080/02626669709492018

Brocca, L., Melone, F., & Moramarco, T. (2011). Distributed rainfall-runoff modelling for flood frequency estimation and flood forecasting. *Hydrological Processes*, *25*(18), 2801–2813. https://doi.org/10.1002/hyp.8042

Brocca, L., Moramarco, T., Melone, F., Wagner, W., Hasenauer, S., & Hahn, S. (2012). Assimilation of Surface- and Root-Zone ASCAT Soil Moisture Products Into Rainfall-Runoff Modeling. *IEEE Transactions on Geoscience and Remote Sensing*, *50*(7), 2542–2555. https://doi.org/10.1109/tgrs.2011.2177468

Francés, F., Vélez, J. I., & Vélez, J. J. (2006). Split-parameter structure for the automatic calibration of distributed hydrological models. *Journal of Hydrology*, *332*(1–2), 226–240. https://doi.org/10.1016/j.jhydrol.2006.06.032

Hansen, N., Müller, S. D., & Koumoutsakos, P. (2003). Reducing the Time Complexity of the Derandomized Evolution Strategy with Covariance Matrix Adaptation (CMA-ES). *Evolutionary Computation*, *11*(1), 1–18. https://doi.org/10.1162/106365603321828970

Massari, C., Camici, S., Ciabatta, L., & Brocca, L. (2018). Exploiting Satellite-Based Surface Soil Moisture for flood forecasting in the Mediterranean Area: State update versus rainfall correction. *Remote Sensing*, *10*(2), 292. https://doi.org/10.3390/rs10020292

Melone, F., Corradini, C., & Singh, V. P. (2002). Lag prediction in ungauged basins: an investigation through actual data of the upper Tiber River valley. *Hydrological Processes*, *16*(5), 1085–1094. https://doi.org/10.1002/hyp.313

Schaefli, B., Hingray, B., Niggli, M., & Musy, A. (2005). A conceptual glacio-hydrological model for high mountainous catchments. *Hydrology and Earth System Sciences*, *9*(1/2), 95–109. https://doi.org/10.5194/hess-9-95-2005

Schaefli, B., Nicótina, L., Imfeld, C., Da Ronco, P., Bertuzzo, E., & Rinaldo, A. (2014). SEHR-ECHO v1.0: a Spatially Explicit Hydrologic Response model for ecohydrologic applications. *Geoscientific Model Development*, *7*(6), 2733–2746. https://doi.org/10.5194/gmd-7-2733-2014

S2. Supplementary figures for the Alaknanda River basin case study

In Fig. S1-S3, it is noteworthy that the linear, time-invariant transformations to calculate $P_{adj,1}$ and PET from P and ET_0, respectively, rescale the magnitude range of climate forcing but do not alter the spatial patterns represented within the basin. This does not apply to precipitation in Scenarios 1B and 1C due to the different adjustment methods.

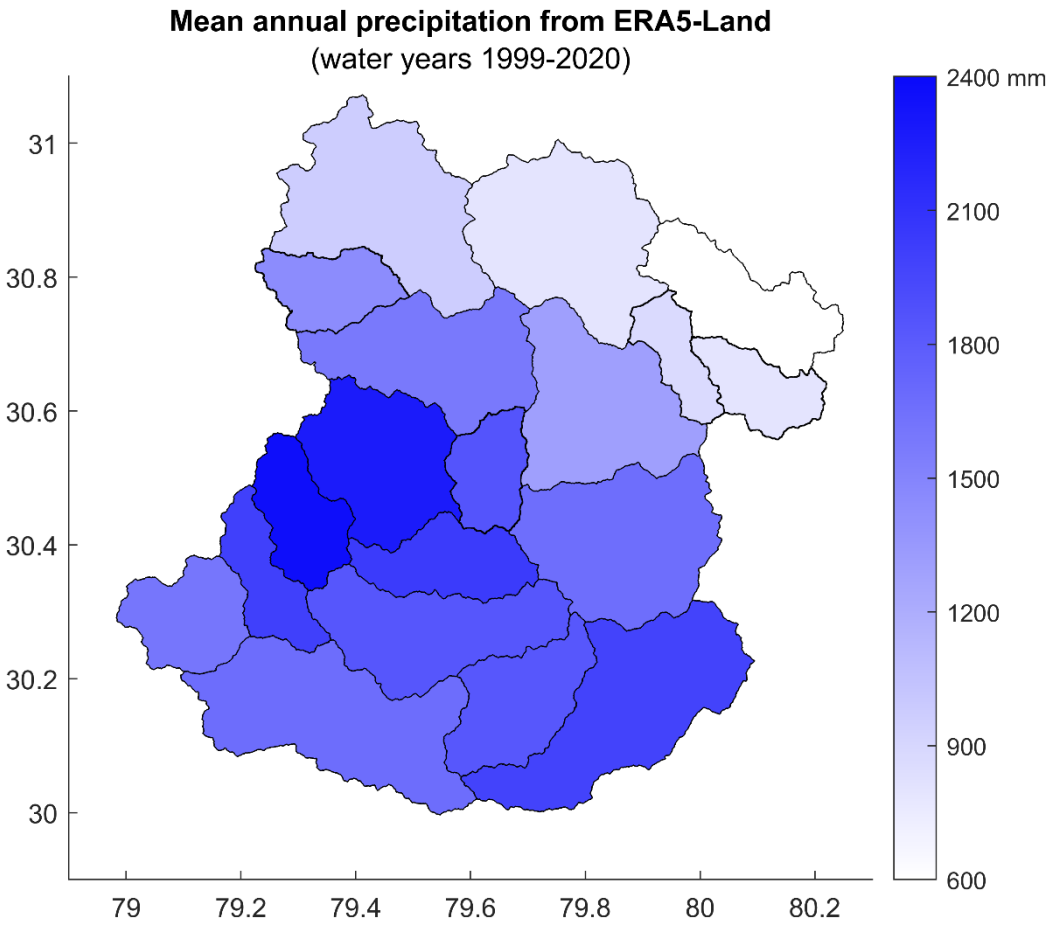

Figure S1. Mean annual precipitation at sub-basin scale, computed from ERA5-Land in the water years 1999-2020.

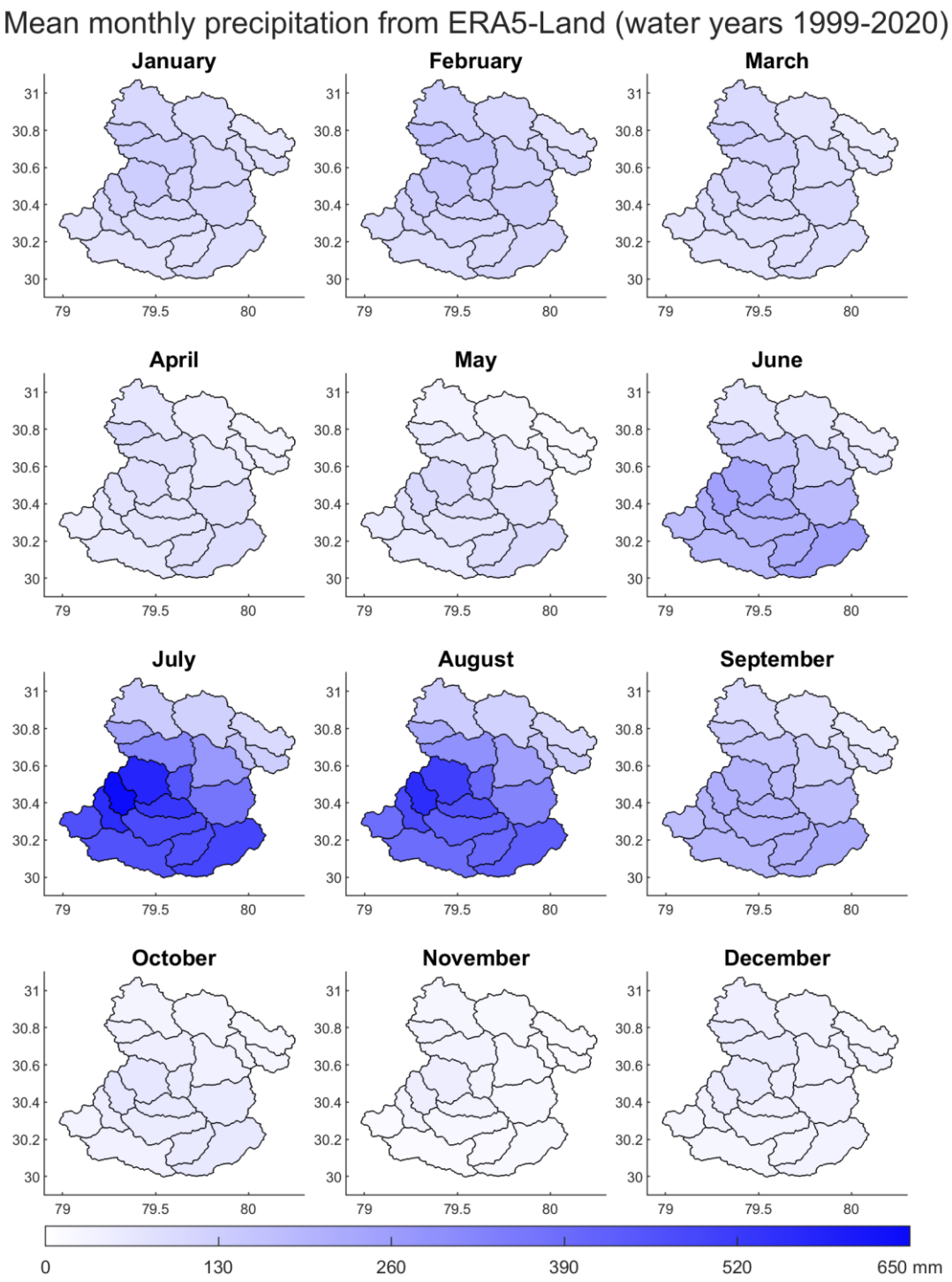

Figure S2. Mean monthly precipitation at sub-basin scale, computed from ERA5-Land in the water years 1999-2020.

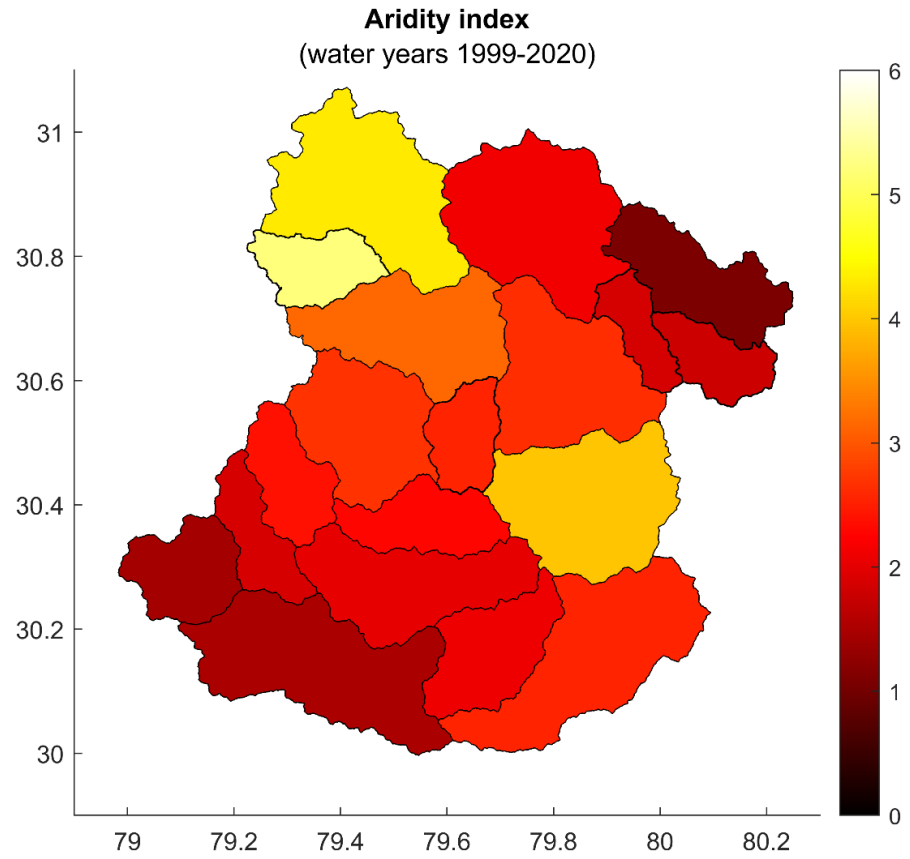

Figure S3. Aridity index at sub-basin scale, computed from ERA5-Land as the ratio of mean annual precipitation to mean annual reference evapotranspiration.

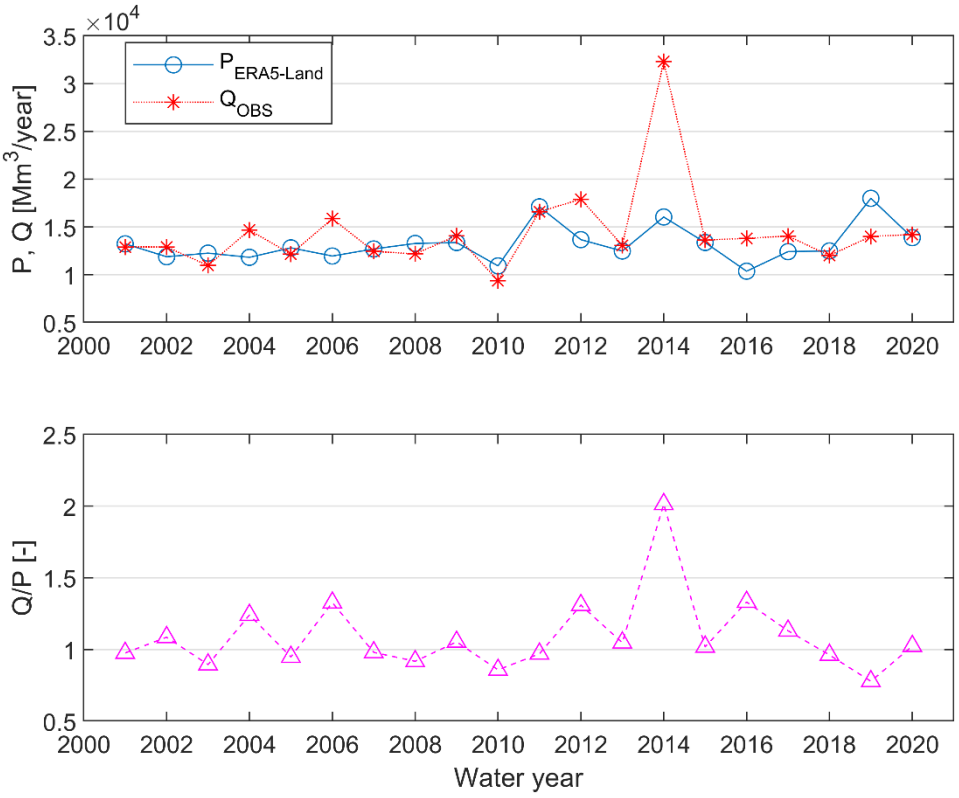

Figure S4. Annual distribution of ERA5-Land precipitation and gauge streamflow volume at basin scale (on the top) and corresponding values of the runoff-to-precipitation ratio (on the bottom).

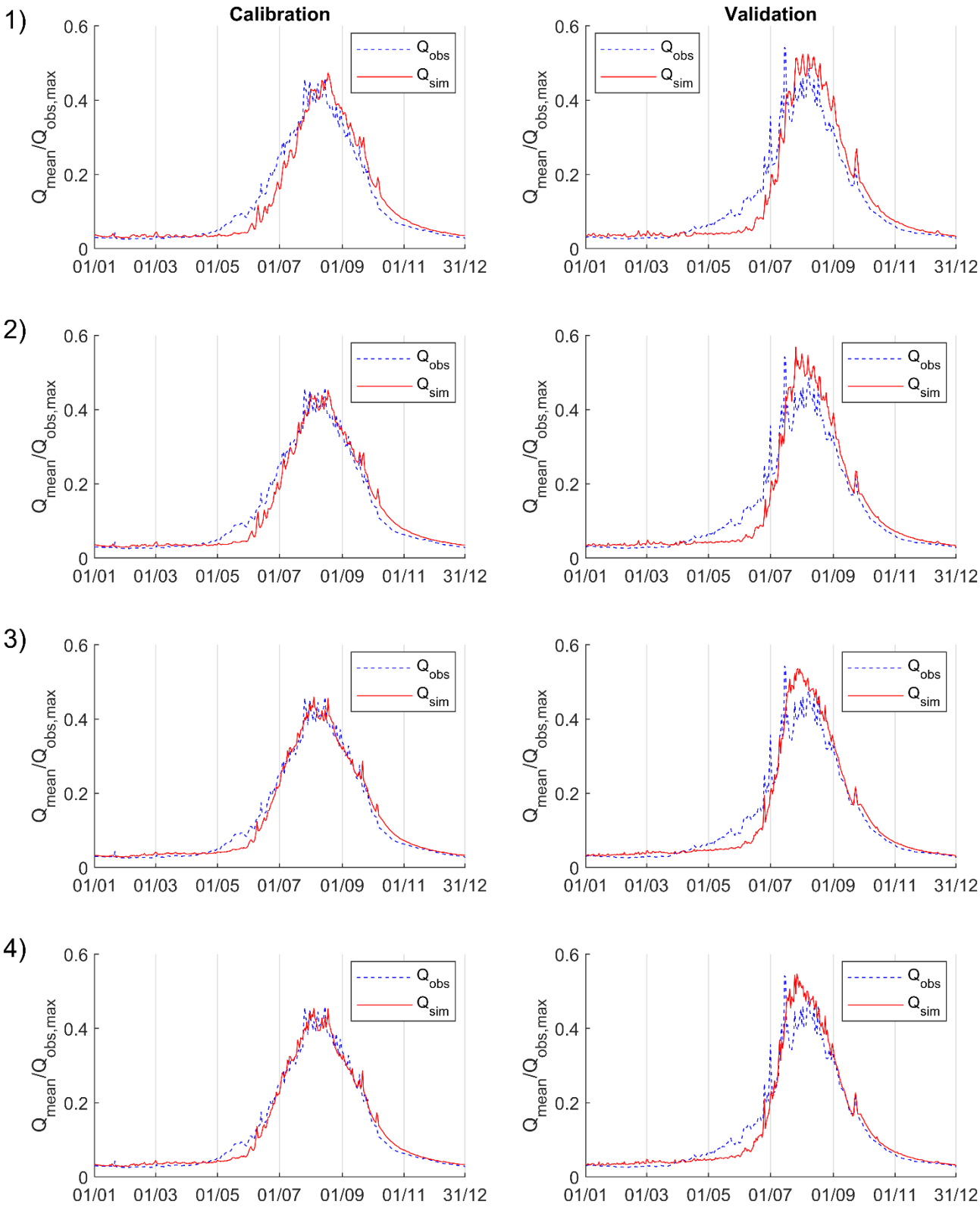

Figure S5: For Scenarios 1) to 4), multi-year mean streamflow for a given day of the year, during calibration (on the left) and validation (on the right) periods. Represented data are normalized with respect to the maximum observed streamflow value.

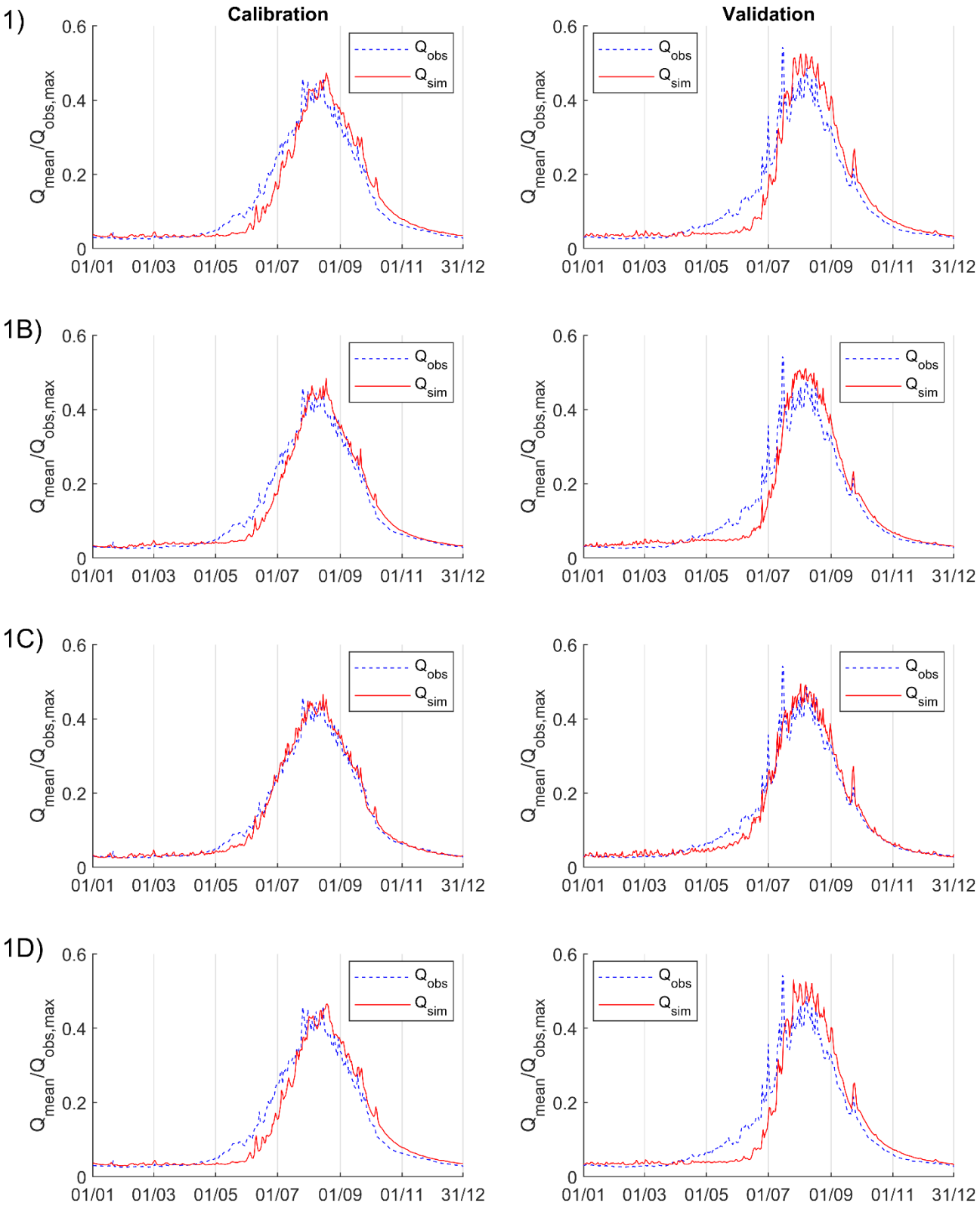

Figure S6. For Scenario 1 and its variants (1B, 1C, and 1D), multi-year mean streamflow for a given day of the year, during calibration and validation periods. Represented data are normalized with respect to the maximum observed streamflow value.

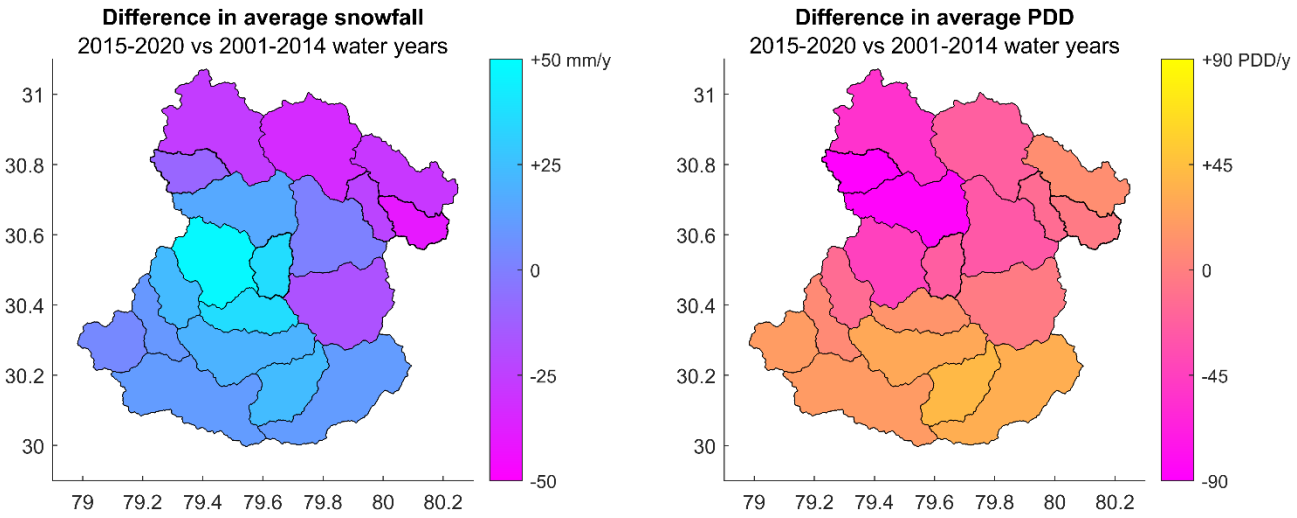

Figure S7. Spatial distribution of difference in mean annual solid precipitation (on the left) and positive-degree-days, PDD (on the right), between validation and calibration periods, derived from ERA5-Land reanalysis.

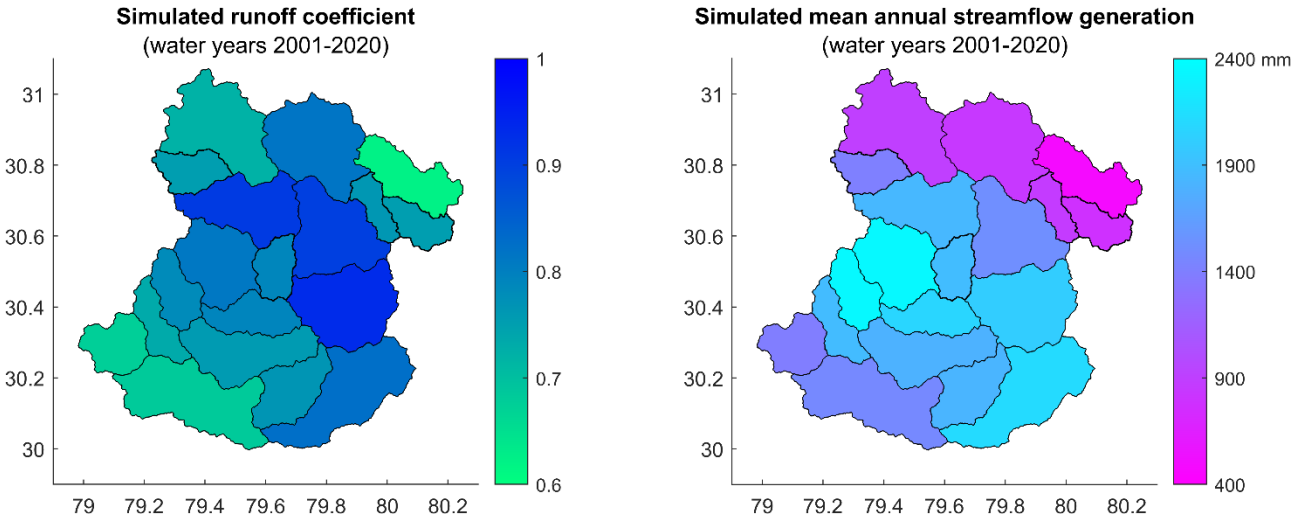

Figure S8. Spatial distribution of simulated runoff coefficient (on the left) and mean annual streamflow generation (on the right), over the study period for Scenario 1. In both panels, streamflow benefits from the contribution of glacier melt in addition to that of precipitation.